HEAVY FLAVOUR PRODUCTION AND SPECTROSCOPY*

Maddalena Frosini

INFN and University of Florence
P.zza S. Marco, 4, 50121 Florence, Italy

(Received April 16, 2013)

This contribution is a summary of the main measurements performed by the LHCb Collaboration in the heavy flavour physics sector and regarding both the production and the spectroscopy. The measurements presented here use the data sample acquired by the experiment from 2010 and 2012 at a collision energy of $\sqrt{s} = 7$ TeV and $\sqrt{s} = 8$ TeV in the centre of mass. Outlooks for ongoing and future measurements are also given.

DOI:10.5506/APhysPolB.44.1441
PACS numbers: 13.25.Hw, 14.40.Pq, 14.40.Lb, 14.20.Mr

1. Introduction

Studies of the heavy quark production mechanism in hadronic collisions provide powerful tests of QCD predictions [1]. Looking, for example, at the heavy quarkonia states, the production can be factorized in two steps according to the QCD. The $q\overline{q}$ pair is firstly produced through small-distance interaction and it then evolves towards the final state. Many theoretical models have been proposed to describe the quarkonium production mechanism and the most important ones are the Color Singlet (CS) and Color Octet (CO) models. The CS model [2, 3] predicts the production of the $q\overline{q}$ pair directly in the color singlet state and the angular momentum and spin number are maintained during the evolution. In the CO model [4], based on a non-relativistic QCD approach, the probability of evolution of the $q\overline{q}$ pair in the final state is given by the color octet matrix terms. The CS prediction underestimates the J/ψ differential cross section measurement provided by CDF [5] but by introducing the color octet terms, the shape and the magnitude are reproduced. Anyway, it is necessary to look also at

* Presented at the Cracow Epiphany Conference on the Physics After the First Phase of the LHC, Kraków, Poland, January 7–9, 2013.

other observables to better understand the production scenario. Thanks to the excellent capability, the LHCb is contributing with different measurement in understanding the production mechanism as well as the spectra of the different heavy quark states.

2. The LHCb detector

The LHCb detector [6], shown in Fig. 1, is a single-arm forward spectrometer covering the pseudo-rapidity range $2 < \eta < 5$, designed for the study of hadrons containing b or c quarks. The LHCb detector includes a high precision tracking system consisting of a silicon-strip vertex detector surrounding the proton–proton interaction region, a large-area silicon-strip detector located upstream of a dipole magnet with a bending power of about 4 Tm, and three stations of silicon-strip detectors and straw drift-tubes placed downstream. The combined tracking system has a momentum resolution $\delta p/p$ that varies from 0.4% at 5 GeV/c to 0.6% at 100 GeV/c, and an impact parameter resolution of 20 μm for tracks with high transverse momentum. Charged hadrons are identified using two ring-imaging Cherenkov detectors. Photon, electron and hadron candidates are identified by a calorimeter system consisting of scintillating-pad and pre-shower detectors, an electromagnetic calorimeter and a hadron calorimeter. Muons

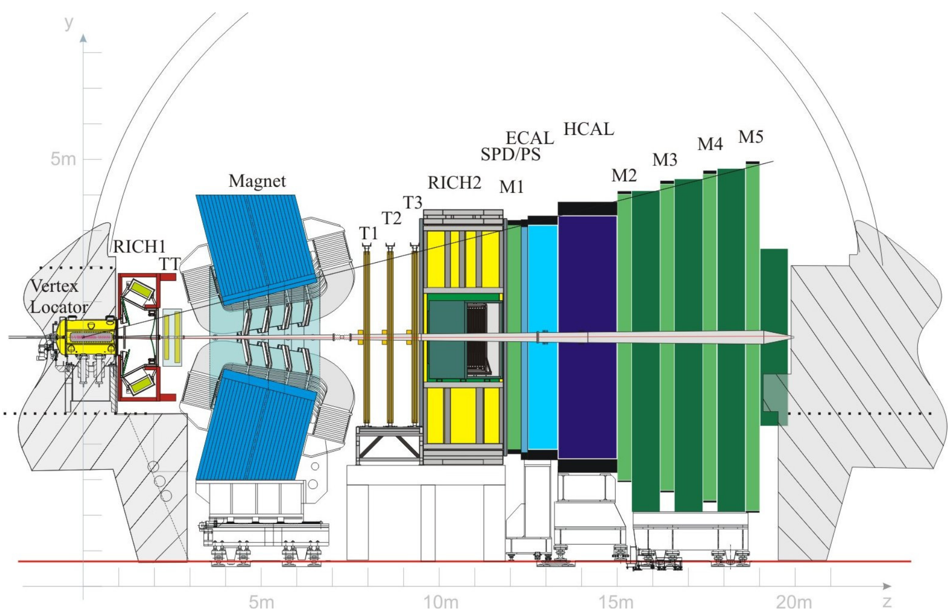

Fig. 1. yz view of the LHCb detector.

are identified by a muon system composed of alternating layers of iron and multiwire proportional chambers. The trigger consists of a hardware stage, based on information from the calorimeter and muon systems, followed by a software stage which applies a full event reconstruction.

3. J/ψ cross section measurement

The cross section is measured analysing the J/ψ meson decaying in two muons: the data sample corresponds to an integrated luminosity $\mathcal{L} = (5.2 \pm 0.5)$ pb^{-1} of pp collisions at $\sqrt{s} = 7$ TeV recorded by the experiment in the 2010. The double differential cross section in J/ψ p_{T} and y is measured using the following formula:

$$\frac{d^2\sigma}{dp_{\mathrm{T}}dy} = \frac{N(J/\psi \to \mu^+\mu^-)}{L \times \varepsilon_{\mathrm{tot}} \times \mathcal{B}(J/\psi \to \mu^+\mu^-)\Delta p_{\mathrm{T}}\Delta y}\,, \tag{1}$$

where $N(J/\psi \to \mu^+\mu^-)$ is the number of selected J/ψ decaying in two muons, $\mathcal{L}$ is the integrated luminosity, $\varepsilon_{\mathrm{tot}}$ is the total efficiency (estimated from Monte Carlo including the detector acceptance, the reconstruction and trigger efficiency), $\mathcal{B}(J/\psi \to \mu^+\mu^-)$ is the branching ratio of the $J/\psi \to \mu^+\mu^-$ decay, Δp_{T} and Δy are, respectively, the J/ψ transverse momentum and rapidity bin sizes. The analysis selection requires at least one reconstructed primary vertex in each event. The J/ψ candidates are formed from pairs of opposite sign charged tracks reconstructed in the tracking system and identified as muons. The two muons must have a good quality of the track fit and originate from a common vertex. To separate the prompt and the delayed component, the J/ψ pseudo-proper time is used, defined as $t_z = \frac{(z_{J/\psi}-z_{\mathrm{PV}})m_{J/\psi}}{p_z}$, where $z_{J/\psi}$ and z_{PV} are the J/ψ decay vertex and the primary vertex positions along the beam axis and $m_{J/\psi}$ and p_z are, respectively, the mass and the momentum component of the J/ψ along the beam axis. Figures 2 and 3 show, respectively, the double differential prompt cross section and the differential prompt cross section integrated over rapidity as a function of p_{T}. Results are compared with the prediction of three different theoretical models (Colour Singlet model, Colour Octet model and Colour Evaporation model). In Fig. 4, the double differential cross section of the delayed component is shown and in Fig. 5, it is integrated over rapidity and compared with the fixed order with next-to-leading-log resummation (FONLL, [7, 8]) computation. The total integrated cross sections are

$$\begin{aligned} \sigma_{\mathrm{prompt}} &= 10.52 \pm 0.04(\mathrm{stat}) \pm 1.40(\mathrm{sys})^{+1.64}_{-2.20}(\mathrm{pol})\,\mu\mathrm{b}\,, & (2)\\ \sigma_{\mathrm{delayed}} &= 1.14 \pm 0.01(\mathrm{stat}) \pm 0.16(\mathrm{sys})\,\mu\mathrm{b}\,. & (3) \end{aligned}$$

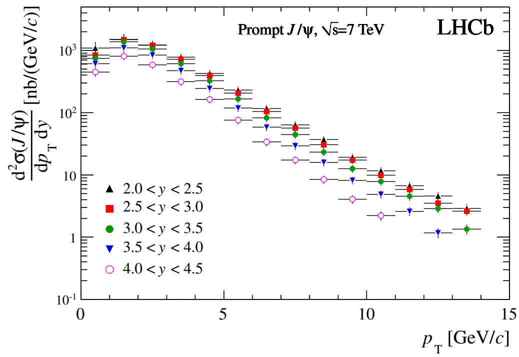

Fig. 2. Double differential cross section of J/ψ prompt component.

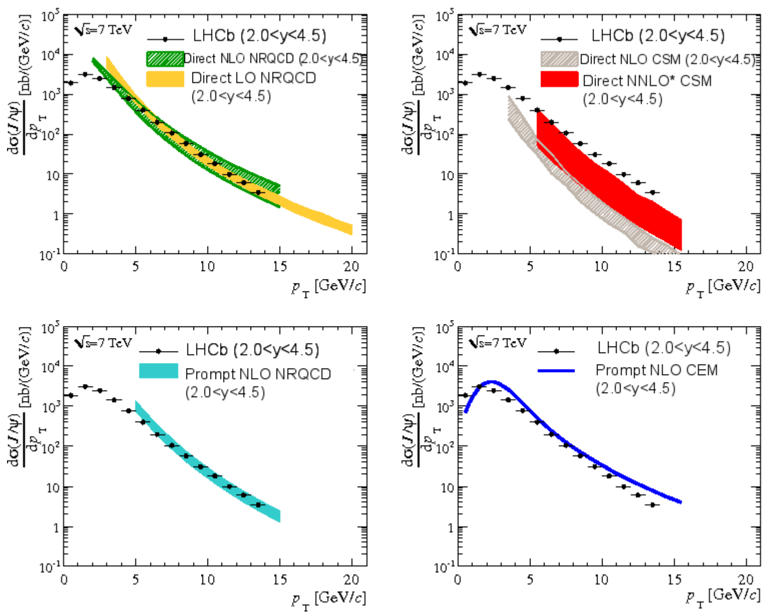

Fig. 3. Prompt J/ψ differential cross section compared with different theoretical models. The top plots show the direct component only and the bottom ones include the feed down.

The first and the second uncertainties are the statistical and the systematic, where the main sources of systematic uncertainty come from the luminosity measurement, the tracking and trigger efficiency. The third uncertainty on the prompt cross section is due to the unknown polarization of the J/ψ and it is estimated calculating the total efficiency in two possible extreme scenarios of fully transverse and fully longitudinal polarization. The deviation from

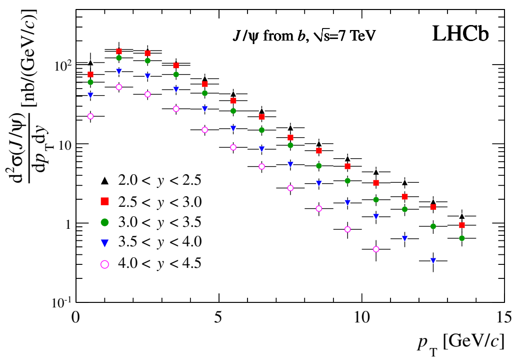

Fig. 4. Double differential cross section of the delayed J/ψ component.

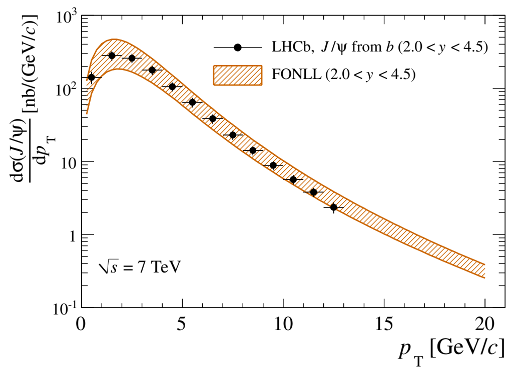

Fig. 5. Differential cross section of delayed J/ψ component compared with FONLL computation.

the case of zero polarization is assigned as systematic uncertainty to the measurement. From Eq. (3) the $b\bar{b}$ cross section is extrapolated to the full solid angle using the formula

$$\sigma\left(pp \to b\bar{b}X\right) = \alpha_{4\pi}\frac{\sigma_{\text{delayed}}}{2\mathcal{B}(b \to J/\psi X)} = 288 \pm 4(\text{stat}) \pm 48(\text{sys})\ \mu\text{b}\,. \quad (4)$$

All these results have been published in Ref. [9].

Using the same strategy, the J/ψ differential and total inclusive cross section has been measured also with 70.6 nb^{-1} of pp collisions taken at 2.76 TeV in the centre of mass [10]. The result for the differential cross section is shown in Fig. 6 as a function of J/ψ p_{T}. The integrated cross section has also been estimated in the analysis range, $2.0 < y < 4.5$ and $p_{\text{T}} < 12$ GeV$/c$,

$$\sigma_{\text{inclusive J}/\psi} = 5.6 \pm 0.1(\text{stat}) \pm 0.4(\text{syst})\ \mu\text{b}\,. \quad (5)$$

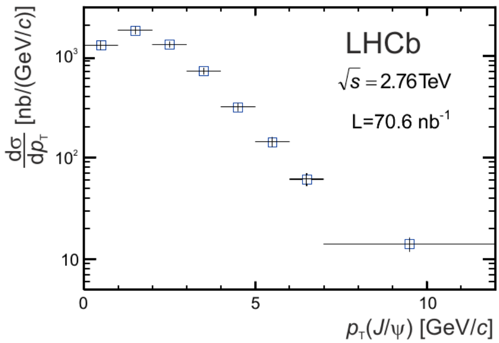

Fig. 6. Differential cross section of the inclusive J/ψ.

4. χ_c production

The study of the J/ψ production through the radiative decays of the χ_c states provides a useful test of both the Color Singlet and Color Octet model. It is fundamental also for the J/ψ polarization measurement: in fact, the directly produced J/ψ and those coming from χ_c decays can carry different polarization and this represents a possible source of uncertainty for the polarization measurement of the prompt J/ψ component. The knowledge of the fraction of J/ψ coming from χ_c decays can help to quantify this uncertainty.

The relative cross section $\sigma(\chi_{c2})/\sigma(\chi_{c1})$ is measured using two different data samples of 37 pb^{-1} [11] and 370 pb^{-1} [12], acquired by the LHCb experiment during the 2010 and 2011, respectively. In both cases, the χ_c states are identified through their radiative decay $\chi_c \to J/\psi\gamma$ with the J/ψ decaying to two muons $J/\psi \to \mu^+\mu^-$. For the first measurement, with a smaller data sample, χ_c states have been reconstructed using photons detected in the calorimeter system. This allows to have a higher statistics but the poor resolution of the calorimeter does not permit to have a good separation between the two χ_{c1} and χ_{c2} states. In the second measurement, the photons converted in the detector material before the magnet have been used, $\gamma \to e^+e^-$. In this way, it is possible to resolve the two states taking advantage of the good resolution of the tracker, as it is shown in Fig. 7 (χ_{c1} and χ_{c2} components are shown, respectively, in dark and light grey).

In both measurements, the efficiency is determined from the Monte Carlo simulation and the number of signal events is extracted with a fit to the invariant mass difference spectra, in four bins of J/ψ transverse momentum.

The results for the relative cross section $\sigma(\chi_{c2})/\sigma(\chi_{c1})$ are shown in Fig. 8. In the plot, the inner error bars correspond to the statistical uncertainties and the outer bars correspond to the sum of all the sources of systematic uncertainties. The shaded area represents the maximum effect

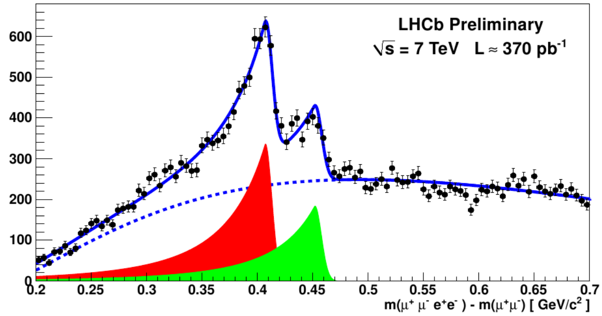

Fig. 7. Invariant mass difference spectrum $\Delta m = m(\chi_c) - m(J/\psi) = m(e^+e^-\mu^+\mu^-) - m(\mu^+\mu^-)$ using converted photons.

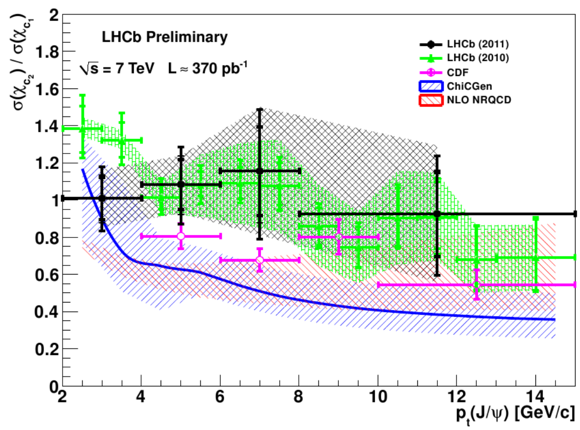

Fig. 8. Relative cross section $\sigma(\chi_{c2})/\sigma(\chi_{c1})$ in bins of J/ψ transverse momentum.

due to the unknown χ_c polarization. In green triangles and black full points the results obtained reconstructing the photons in the calorimeter (2010 statistics) and the converted photons (2011 statistics) are shown. The results from the CDF collaboration are shown in magenta (empty circles) [13]. The blue (oblique lines from bottom left to top right) and red (oblique lines from bottom right to top left) shaded area correspond to the Color Singlet ([14]) and NRQCD ([15]) prediction respectively.

The χ_c to J/ψ ratio has been measured with the 36 pb^{-1} data sample acquired by the experiment in the 2010 [16]. The χ_c states are reconstructed through their radiative decay $\chi_c \to J/\psi\gamma$ with the J/ψ decaying into two muons $J/\psi \to \mu^+\mu^-$. The results are shown in Fig. 9, compared with the CDF measurement and with two theoretical models, the Color Singlet (blue oblique lines from top left to bottom right, [14]) and NRQCD approach (red oblique lines from bottom left to top right, [15]).

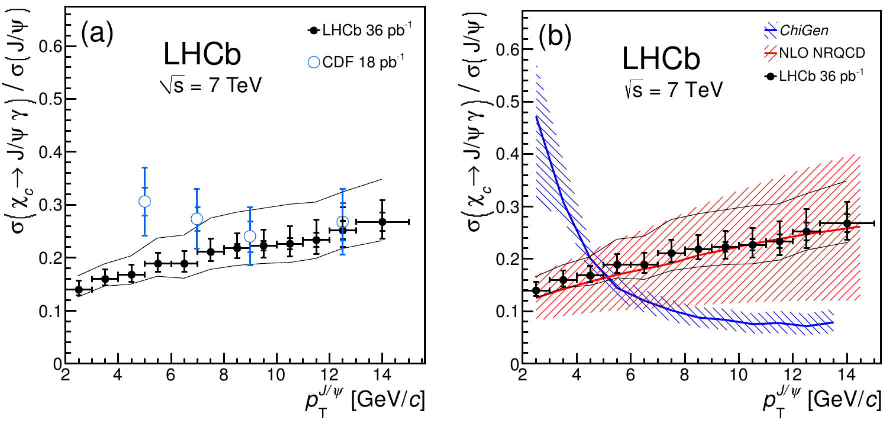

Fig. 9. Relative cross section $\sigma(\chi_c)/\sigma(J/\psi)$ in bins of J/ψ transverse momentum. The results (black points) are compared with the CDF measurement [17] and with the Color Singlet ([14]) and Color Octet ([15]) prediction (respectively the blue and red area.)

5. Double charm production

Recently, the double charmonium and the charmonium production in association with an open charm have been suggested as a probe of the production mechanism. In the pp collisions also other mechanisms, as the Double Parton Scattering (DPS, [18–20]), can be involved in the production and their contribution can be estimated with respect to the Single Parton Scattering (SPS, [21–23]).

Such a study has been performed at the LHCb through the measurement of the double J/ψ, published in Ref. [24], and the double charm production involving an open charm hadron (such as D^0, D^+, D_s^+ and Λ_c^+) [25], with the 2010 and 2011 datasets (respectively 37 pb^{-1} and 355 pb^{-1}).

The signal yield is determined with a fit to the invariant mass distribution of the first muon pair in bins of the second muon pair and correcting the number of signal events by the total efficiency.

The total efficiency can be factorized in three different terms

$$\varepsilon^{\rm tot}_{J/\psi J/\psi} = \varepsilon^{\rm sel\&reco\&acc}_{J/\psi J/\psi} \times \varepsilon^{\mu{\rm ID}}_{J/\psi J/\psi} \times \varepsilon^{\rm trg}_{J/\psi J/\psi}\,, \qquad (6)$$

where $\varepsilon^{\rm sel\&reco\&acc}_{J/\psi J/\psi}$ is the acceptance, selection and reconstruction efficiency, $\varepsilon^{\mu{\rm ID}}_{J/\psi J/\psi}$ is the muon identification efficiency and $\varepsilon^{\rm trg}_{J/\psi J/\psi}$ is the trigger efficiency. To take into account the distortion due to the unknown J/ψ polarization, $\varepsilon^{\rm sel\&reco\&acc}_{J/\psi J/\psi}$ is a function of the J/ψ $\cos\theta$, where θ is the angle between the μ^+ in the J/ψ center of mass frame and the Lorentz boost from the laboratory frame to the J/ψ frame.

The corrected invariant mass distribution of the first muon pair in bins of the second muon pair is shown in Fig. 10, in three bins of J/ψ transverse momentum in a particular bin of rapidity.

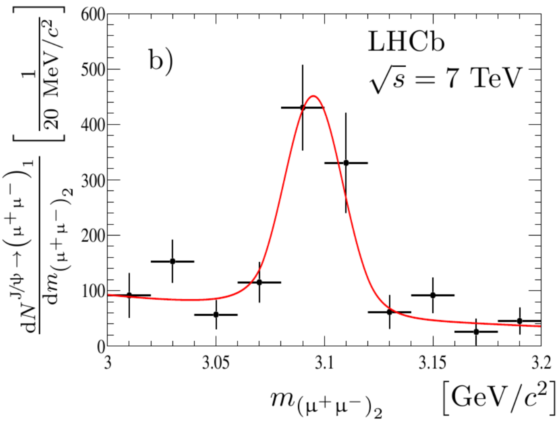

Fig. 10. Invariant mass distribution of the first muon pair in bins of the second muon pair for the double J/ψ production.

The double J/ψ production cross section has been measured reconstructing the two J/ψ mesons in their decay to two muons. Both the J/ψ mesons have been required to have rapidity and transverse momentum lying, respectively, in the ranges $2.0 < y < 4.5$ and $p_{\mathrm{T}} < 10$ GeV$/c$. The double J/ψ cross section is estimated to be

$$\sigma_{J/\psi J/\psi} = \frac{N^{\mathrm{corr}}_{J/\psi J/\psi}}{\mathcal{L}\,\mathcal{B}^2(J/\psi \to \mu^+\mu^-)} = 5.1 \pm 1.0(\mathrm{stat}) \pm 1.1(\mathrm{sys})\ \mathrm{nb}\,, \tag{7}$$

where $N^{\mathrm{corr}}_{J/\psi J/\psi}$ is the efficiency corrected signal yield, $\mathcal{L} = 37\ \mathrm{pb}^{-1}$ is the integrated luminosity and $\mathcal{B}(J/\psi \to \mu^+\mu^-)$ is the branching ratio of the J/ψ decay into a muon pair.

The first and second uncertainty are, respectively, statistical and systematic. The main contributions to the systematic uncertainty come from the tracking and trigger efficiency and from the unknown J/ψ polarization.

The experimental result obtained by the LHCb has been compared with the theoretical contribution calculated in color-singlet model, from the SPS and the DPS. The two contributions, estimated in the LHCb acceptance, are listed together with the related uncertainties in Table I [24]. The sum of the two contributions is in agreement with the experimental value reported in Eq. (5), but the uncertainties on the theoretical expectations are still too large to draw a definite conclusion on the production mechanism.

TABLE I

SPS and DPS contribution to the double J/ψ production cross section estimated in the LHCb acceptance. The theoretical uncertainties are also listed.

Model	Cross section [nb]	Uncertainty
Single Parton S.	4.15	30%
Double Parton S. contribution	2	50%

The production cross sections of double charm, involving an open charm hadron, D^0, D^+, D_s^+ or Λ_c^+ have been measured using 355 pb^{-1} out of the 2011 datasets. The J/ψ, D^0, D^+, D_s^+ and Λ_c^+ hadrons have been reconstructed through the following decays: $J/\psi \to \mu^+\mu^-$, $D^0 \to \pi^+K^-$, $D^+ \to \pi^+\pi^+K^-$, $D_s^+ \to \pi^+K^+K^-$, $\Lambda_c^+ \to p\pi^+K^-$.

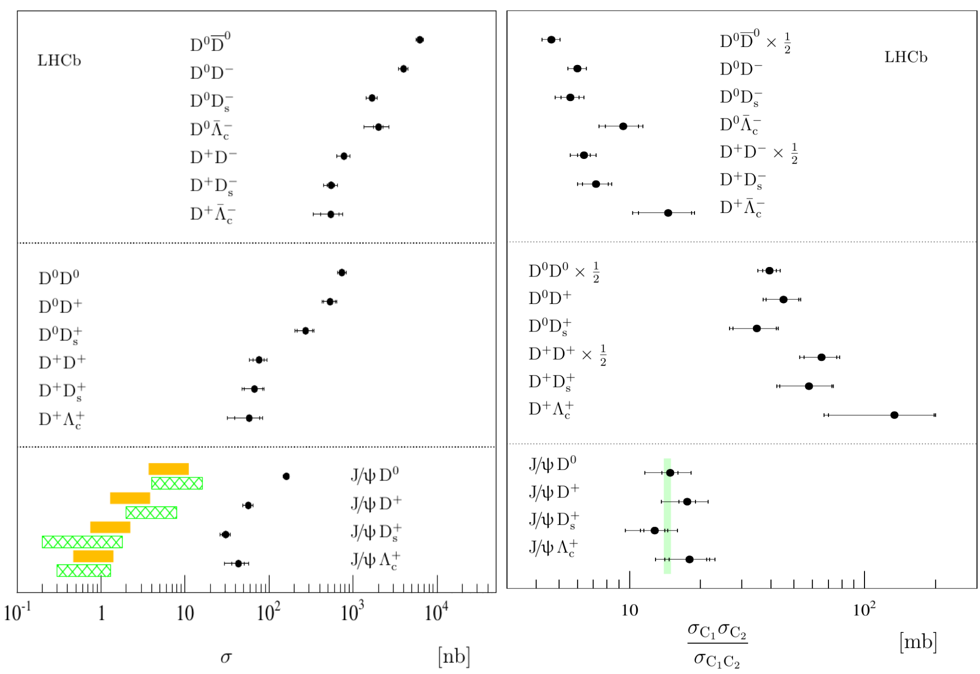

Fig. 11. (a) Double open charm production cross section. The experimental results (black points) are compared with the gluon–gluon fusion expectation (grey/yellow and hatched/green areas [21–23]). (b) Results for the prompt open charm cross sections and double open charm cross section ratio compared with the theoretical expectation computed with the DPS approach [18–20].

In Fig. 11(a) [25], the results for the production cross section of the double charm processes are shown, compared with the theoretical expectation estimated with gluon–gluon fusion model. In Fig. 11(b) [25], the ratios of the product of the prompt open charm cross sections and the double open charm cross section show a good agreement with the theoretical expectation from the DPS, assuming the effective cross section measured in multi-jet events at Tevatron [26]. In the plots, the inner error bars represent the statistical uncertainties while the outer error bars are the sum in quadrature of the statistical and systematic uncertainties.

6. Open charm cross section

The measurements of the production cross sections of charmed hadrons can provide useful tests for the QCD hadronization and fragmentation functions. The measurements performed by the CDF Collaboration in $p\overline{p}$ collisions at $\sqrt{s} = 1.96$ TeV energy in the centre of mass and by the ALICE Collaboration in pp collisions at $\sqrt{s} = 2.96$ TeV and $\sqrt{s} = 7$ TeV energy show a good agreement with the Generalized Mass Variable Flavour Number Scheme (GMVFNS, [27]) and the Fixed Order with Next-to-Leading-Log resummation (FONLL, [28]) models in the low rapidity region. The LHCb can explore the very forward rapidity region thanks to the geometry of the detector.

At the LHCb the D^0, D^+, D^{*+}, D_s^+ and Λ_c^+ production cross sections have been measured with 15 nb^{-1} of pp collisions taken by the experiment in 2010 at $\sqrt{s} = 7$ TeV. The analysis is based on the fully reconstructed decays of the charmed hadrons in the following modes: $D^0 \to \pi^+K^-$, $D^+ \to \pi^+\pi^+K^-$, $D_s^+ \to \phi(K^+K^-)\pi^+$, $D^{*+} \to D^0\pi^+$ and $\Lambda_c^+ \to p\pi^+K^-$. The measurements are performed in eight bins of p_{T} and five bins of rapidity y of the charmed hadrons in the range 0 GeV$/c < p_{\mathrm{T}} < 8$ GeV$/c$ and $2.0 < y < 4.5$ except for the Λ_c^+. Due to the limited statistics for this measurement, the sample has been binned in two ways: in the range 2 GeV$/c < p_{\mathrm{T}} < 8$ GeV$/c$ the data sample has been split in six bins of p_{T} and a unique bin of rapidity $2.0 < y < 4.5$, while in the range 0 GeV$/c < p_{\mathrm{T}} < 2$ GeV$/c$ the sample has been split in a unique bin of p_{T} and five uniform bins of rapidity. The results for the double differential cross sections are shown in Figs. 12, 13, and 14 compared to the theoretical predictions obtained by the GMVFNS and FONLL models. The experimental points and the theoretical curves in different y regions are scaled by factors 10^{-m} for a better visualization, where m is plotted together with the corresponding y bin. The shaded regions are the theoretical uncertainties on the GMVFNS prediction. The error bars are the sum in quadrature of statistical and systematic uncertainties.

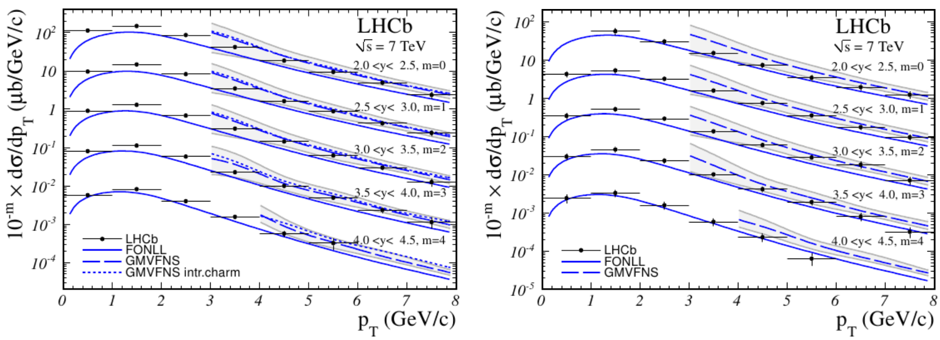

Fig. 12. Differential cross section of D^0 (left) and D^+ (right) compared with the theoretical predictions.

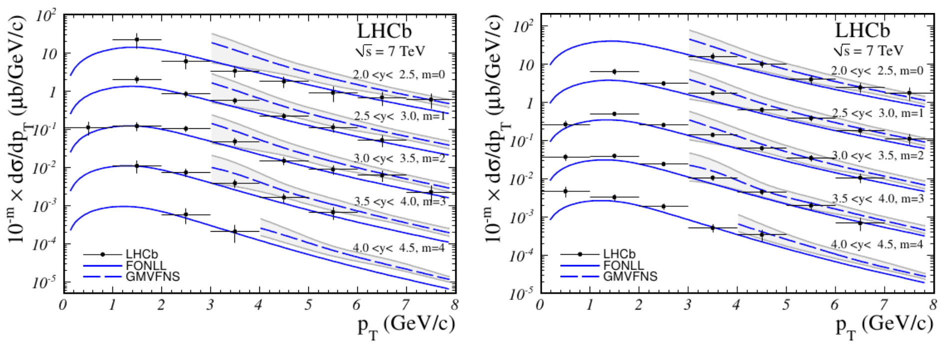

Fig. 13. Differential cross section of D_s^+ (left) and D^{*+} (right) compared with the theoretical predictions.

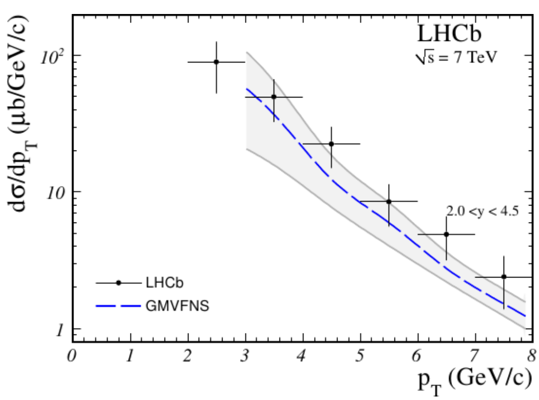

Fig. 14. Differential cross section of Λ_c^+ compared with the theoretical predictions.

The total $c\bar{c}$ cross section has been also estimated combining the five measurements extrapolated with the corresponding fragmentation function:

$$\sigma(c\bar{c})_{p_{\rm T}<8\,{\rm GeV}/c,\,2.0<y<4.5} = 1419 \pm 12({\rm stat}) \pm 116({\rm sys}) \pm 65({\rm frag})\,\mu{\rm b}\,, \quad (8)$$

where the uncertainties are, respectively, statistical, systematic and due to the fragmentation functions.

7. Λ_b production and excited states

The b-baryons production has not been deeply studied in the past years. The CMS Collaboration recently published the first measurement of the production cross section of the Λ_b^0 in the fully reconstructed decay $\Lambda_b^0 \to J/\psi\Lambda$ for $p_{\rm T} > 10$ GeV/c and $|y| < 2.0$ (Ref. [29]).

The LHCb recently presented a preliminary result on the Λ_b^0 in the decay channel $\Lambda_b^0 \to J/\psi\Lambda$, with $J/\psi \to \mu^+\mu^-$ in the complementary region $p_{\rm T} < 13$ GeV/c and $2.2 < y < 4.5$ [30]. The measurement is based on the 36 pb^{-1} of pp collisions at $\sqrt{s} = 7$ TeV in the centre of mass recorded by the experiment in 2010. The data sample has been split in eight categories according to the b quark content, magnet polarity and the track type. The results are shown in Fig. 15. The experimental points are shown in stars (red) for each one of the different categories. The thin (black) and thick (red) error bars are, respectively, the statistical and systematic uncertainties. The two bands (shaded green area) are the Λ_b^0 and $\overline{\Lambda}_b^0$ average and the horizontal wavy (red) line is the prediction from the LHCb simulation. The integrated results for the Λ_b^0 and $\overline{\Lambda}_b^0$ are, respectively,

$$\sigma_{\Lambda_b^0} \times \mathcal{B}(\Lambda_b \to \Lambda^0\ J/\psi) = 4.08 \pm 0.59({\rm stat}) \pm 0.36({\rm sys})\,\mu{\rm b}\,, \quad (9)$$

$$\sigma_{\overline{\Lambda}_b^0} \times \mathcal{B}(\overline{\Lambda}_b \to \overline{\Lambda}^0 J/\psi) = 2.60 \pm 0.46({\rm stat}) \pm 0.26({\rm sys})\,\mu{\rm b}\,. \quad (10)$$

Two new excited Λ_b states have also been observed recently at the LHCb in the decay mode $\Lambda_b^0\pi^+\pi^-$, on a data sample of 1 fb^{-1} [31]. The measured masses are:

$$M_{\Lambda_b^{0*}(5912)} = 5911.97 \pm 0.12({\rm stat}) \pm 0.02({\rm sys}) \pm 0.66\left(\Lambda_b^0{\rm mass}\right)\ {\rm MeV}/c^2\,, \quad (11)$$

$$M_{\Lambda_b^{0*}(5920)} = 5919.77 \pm 0.08({\rm stat}) \pm 0.02({\rm sys}) \pm 0.66\left(\Lambda_b^0{\rm mass}\right)\ {\rm MeV}/c^2 \quad (12)$$

with, respectively, 5.2σ and 10.2σ significance. The uncertainties are, respectively, statistical, systematic and due to the imperfect knowledge of the Λ_b^0 mass. The invariant mass distribution of the $\Lambda_b^0\pi^+\pi^-$ combinations is shown in Fig. 16. The values of the mass difference with respect to the Λ_b^0 have also been calculated and the results are:

$$\Delta M_{\Lambda_b^{0*}(5912)} = 292.60 \pm 0.12(\text{stat}) \pm 0.04(\text{sys})\ \text{MeV}/c^2\,, \qquad (13)$$

$$\Delta M_{\Lambda_b^{0*}(5920)} = 300.40 \pm 0.08(\text{stat}) \pm 0.04(\text{sys})\ \text{MeV}/c^2\,, \qquad (14)$$

where the uncertainty on the Λ_b^0 mass is mostly cancelled out and the remaining part is included in the systematic.

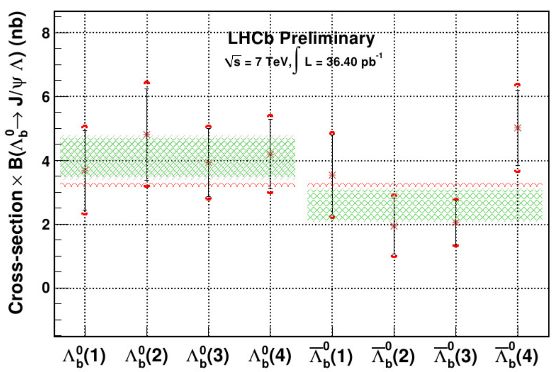

Fig. 15. Production cross section of Λ_b^0 and $\overline{\Lambda}_b^0$ in each one of the eight subsamples compared with the prediction from the LHCb simulation.

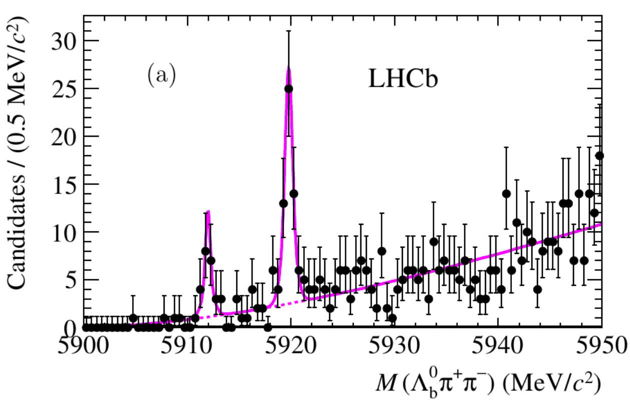

Fig. 16. Invariant mass distribution of $\Lambda_b^0\pi^+\pi^-$ combinations. Black points are the data and the solid line is the fit result.

8. Conclusion

The LHCb has provided many contributions in the heavy flavour sector. A few selected results, based on the data recorded in the past three years have been presented in this report. More results are expected to come in the heavy flavour sector, concerning both the production and the spectra of the states.

REFERENCES

[1] N. Brambilla *et al.*, *Eur. Phys. J.* **C71**, 1534 (2011).
[2] E.L. Berger, D. Jones, *Phys. Rev.* **D23**, 1521 (1981).
[3] R. Baier, R. Rückl, *Phys. Lett.* **B102**, 364 (1981).
[4] G.T. Bodwin, E. Braaten, G.P. Lepage, *Phys. Rev.* **D51**, 1125 (1995).
[5] The CDF Collaboration, *Phys. Rev. Lett.* **79**, 572 (1997).
[6] LHCb Collaboration, *JINST* **3**, S08005 (2008).
[7] M. Cacciari, M. Greco, P. Nason, *J. High Energy Phys.* **9805**, 007 (1998).
[8] M. Cacciari, S. Frixione, P. Nason, *J. High Energy Phys.* **0103**, 006 (2001).
[9] LHCb Collaboration, *Eur. Phys. J.* **C71**, 1645 (2011).
[10] LHCb Collaboration, *J. High Energy Phys.* **1302**, 041 (2013).
[11] LHCb Collaboration, *Phys. Lett.* **B714**, 215 (2012).
[12] LHCb Collaboration, LHCb-CONF-2011-062.
[13] CDF Collaboration, *Phys. Rev. Lett.* **98**, 232001 (2007).
[14] L.A. Harland Lang, W.J. Stirling, `http://projects.hepforge.org/superchic/chigen.html`
[15] Y.-Q. Ma, K. Wang, K.-T. Chao, *Phys. Rev.* **D83**, 111503R (2011).
[16] LHCb Collaboration, *Phys. Lett.* **B718**, 431 (2012).
[17] CDF Collaboration, *Phys. Rev. Lett.* **79**, 578 (1997).
[18] S.P. Baranov, A.M. Snigirev, N.P. Zotov, *Phys. Lett.* **B705**, 116 (2011).
[19] A. Novoselov, `arXiv:1106.2184 [hep-ph]`.
[20] C.H. Kom, A. Kulesza, W.J. Stirling, *Phys. Rev. Lett.* **107**, 082002 (2011).
[21] A.V. Berezhnoy, V.V. Kiselev, A.K. Likhoded, A.I. Onishchenko, *Phys. Rev.* **D57**, 4385 (1998).
[22] S.P. Baranov, *Phys. Rev.* **D73**, 074021 (2006).
[23] J.P. Lansberg, *Eur. Phys. J.* **C61**, 693 (2009).
[24] LHCb Collaboration, *Phys. Lett.* **B707**, 52 (2012).
[25] LHCb Collaboration, `arXiv:1205.0975 [hep-ex]`.
[26] CDF Collaboration, *Phys. Rev.* **D56**, 3811 (1997).
[27] B.A. Kniehl, G. Kramer, I. Schienbein, H. Spiesberger, *Eur. Phys. J.* **C72**, 2082 (2012).

[28] M. Cacciari *et al.*, *J. High Energy Phys.* **1210**, 137 (2012).
[29] CMS Collaboration, *Phys. Lett.* **B714**, 136 (2012).
[30] LHCb Collaboration, LHCb-CONF-2012-031.
[31] LHCb Collaboration, *Phys. Rev. Lett.* **109**, 172003 (2012).